CALIBRATION OF THE OPTICAL MASS PROXY FOR CLUSTERS OF GALAXIES AND AN UPDATE OF THE WHL12 CLUSTER CATALOG

Z. L. WEN, J. L. HAN

National Astronomical Observatories, Chinese Academy of Sciences, 20A Datun Road, Chaoyang District, Beijing 100012, China; zhonglue@nao.cas.cn.
Draft version July 20, 2015

ABSTRACT

Accurately determining the mass of galaxy clusters is fundamental for many studies on cosmology and galaxy evolution. We collect and rescale the cluster masses of 1191 clusters of $0.05 < z < 0.75$ estimated by X-ray or Sunyaev–Zeldovich measurements and use them to calibrate the optical mass proxy. The total r-band luminosity (in units of L^*) of these clusters are obtained by using spectroscopic and photometric data of the Sloan Digital Sky Survey (SDSS). We find that the correlation between the cluster mass M_{500} and total r-band luminosity L_{500} significantly evolves with redshift. After correcting for the evolution, we define a new cluster richness $R_{L*,500} = L_{500} E(z)^{1.40}$ as the optical mass proxy. By using this newly defined richness and the recently released SDSS DR12 spectroscopic data, we update the WHL12 cluster catalog and identify 25,419 new rich clusters at high redshift. In the SDSS spectroscopic survey region, about 89% of galaxy clusters have spectroscopic redshifts. The mass can be estimated with a scatter of 0.17 dex for the clusters in the updated catalog.

Subject headings: galaxies: clusters: general — galaxies: distances and redshifts

1. INTRODUCTION

Clusters of galaxies are the most massive gravitationally bound systems in the universe. Statistics of cluster properties provides very powerful constraints on cosmology and galaxy evolution (see Allen et al. 2011; Wetzel et al. 2012). The cluster mass is a fundamental parameter for galaxy clusters and is related to observational features in the X-ray, optical, millimeter and radio bands (e.g., Voit 2005; Brunetti et al. 2009). Galaxies, intracluster hot gas and dark matter contribute about 5%, 15%, and 80% of the total cluster mass, respectively. Determining the cluster mass is the basis for many studies. For example, the mass function for a complete sample of galaxy clusters can be used to constrain cosmological parameters (e.g., Reiprich & Böhringer 2002; Vikhlinin et al. 2009b; Wen et al. 2010).

Statistics for weak gravitational lensing features is the most direct method to determine the total cluster mass including contributions from member galaxies, hot intracluster gas and dark matter. However, this method requires high-quality image data and also redshift information for faint background galaxies and thus only a few massive clusters have their masses so determined (e.g., Dahle 2006; Bardeau et al. 2007; Okabe et al. 2010; von der Linden et al. 2014b). Based on the assumption that the hot intracluster gas is in hydrostatic equilibrium, the cluster mass can be estimated by using the X-ray surface brightness and temperature distributions (e.g., Finoguenov et al. 2001; Reiprich & Böhringer 2002; Kravtsov et al. 2006; Vikhlinin et al. 2006). A few thousands of galaxy clusters have their masses estimated from the X-ray observables (Vikhlinin et al. 2009a; Mantz et al. 2010; Piffaretti et al. 2011; Takey et al. 2013). In the millimeter band, the thermal Sunyaev–Zeldovich (SZ) effect provides robust mass estimates for more than one thousand massive clusters (Hasselfield et al. 2013; Reichardt et al. 2013; Planck Collaboration et al. 2014), which is independent of cluster dynamical state and redshift (Carlstrom et al. 2002).

The velocity dispersion of member galaxies is certainly a good measure of cluster mass (Girardi et al. 1998), which can be derived from optical spectroscopic data and have been ob-

tained for a limited number of galaxy clusters. However, the spectroscopic observations are usually incomplete for cluster member galaxies, and cluster substructures often induce a bias on the estimated mass (Bird 1995; Sifón et al. 2013). On the other hand, photometric data can be used to identify galaxy clusters (e.g., Koester et al. 2007; Wen et al. 2009; Hao et al. 2010; Szabo et al. 2011; Wen et al. 2012; Oguri 2014; Rykoff et al. 2014). Cluster richness, defined as the total number of member galaxies or their total luminosity, can be used as an optical mass proxy (Popesso et al. 2005, 2007). The challenge is to accurately determine the membership of cluster galaxies by eliminating the contamination by field galaxies. Based on multicolor survey data, the member galaxies can be discriminated by using galaxy colors (e.g., Gladders & Yee 2000; Koester et al. 2007; Hao et al. 2010) or photometric redshifts (e.g., Wen et al. 2009; Szabo et al. 2011). The cluster richness derived from optical photometric data in general is poorly correlated with cluster mass. However, if the correlation is improved, the cluster richness can be used to estimate cluster mass for a very large sample of clusters even up to high redshifts.

The Sloan Digital Sky Survey (SDSS; York et al. 2000) offers an unprecedented photometric data in five broad bands (u, g, r, i, and z) covering 14,000 deg^2 with the exceptional follow-up spectroscopic observations. The photometric data reach a limit of $r = 22.2$ (Stoughton et al. 2002), with the star–galaxy separation reliable to a limit of $r = 21.5$ (Lupton et al. 2001). The spectroscopic survey observes galaxies with a Petrosian magnitude of $r < 17.77$ for the main galaxy sample (Strauss et al. 2002) and a model magnitude $r < 19.9$ for the Luminous Red Galaxy sample (Eisenstein et al. 2001). These galaxies cover a footprint of 10,400 deg^2 in the range of $-11° \leq$ Decl. $\leq 69°$. The latest Data Release 12 (DR12, Alam et al. 2015) includes the photometric data for about 200 million galaxies and the spectroscopic data for about 2.32 million galaxies.

The large samples of galaxy clusters or groups have been identified by using the SDSS spectroscopic data (e.g., Merchán & Zandivarez 2005; Berlind et al. 2006;

Tempel et al. 2014) and the photometric data (e.g., Koester et al. 2007; Wen et al. 2009; Hao et al. 2010; Szabo et al. 2011; Wen et al. 2012; Oguri 2014; Rykoff et al. 2014). Generally, the richness in these cluster catalogs is defined as the total number or the total luminosity of member galaxies, which can be regarded as a coarse mass proxy for clusters up to a redshift of $z \sim 0.4$. At higher redshifts, the discrimination of member galaxies are limited to only very luminous galaxies, and hence the richness is systematically underestimated, as discussed in Wen et al. (2012). We noticed that without a proper calibration, such a cluster richness could be redshift-dependent even at low redshift (e.g., Rozo et al. 2009; Wen et al. 2010).

Many recent samples of galaxy clusters have their masses determined by X-ray or SZ measurements up to redshift of $z \sim 0.75$ (e.g., Piffaretti et al. 2011; Planck Collaboration et al. 2014). These provide an opportunity to calibrate the richness over a large redshift range so that the calibrated richness may be used as a mass proxy for a very large sample of galaxy clusters. In Section 2, we collect the cluster mass in the literature estimated by the X-ray or SZ observations, and for these clusters in the SDSS survey region, we calculate their total r-band luminosity and define a mass proxy that is independent of redshift. On the other hand, the SDSS Baryon Oscillation Spectroscopic Survey (Dawson et al. 2013) offers spectroscopic redshifts for most of the galaxy clusters in the catalog of Wen et al. (2012, i.e., the WHL12 cluster catalog), so that in Section 3 we update the richness and redshift information for the WHL12 clusters, and find new complementary clusters at high redshift.

Throughout this paper, we assume a ΛCDM cosmology, taking $H_0 = 100h$ km s^{-1} Mpc^{-1}, with $h = 0.7$, $\Omega_m = 0.3$ and $\Omega_\Lambda = 0.7$.

2. CALIBRATING THE RICHNESS FOR AN OPTICAL MASS PROXY

We collect the estimated masses of many large samples of galaxy clusters, and then scale them to each other by using common clusters. The scaled masses of the composite sample of galaxy clusters are used to calibrate the optical richness of galaxy clusters in a large range of redshifts so that any redshift dependence can be eliminated.

2.1. *The mass estimates for galaxy clusters and their rescaling between different samples*

Many samples of galaxy clusters have their mass estimated by using the X-ray or SZ measurements (e.g. Kravtsov et al. 2006; Zhang et al. 2008; Pratt et al. 2009; Zhao et al. 2013). To make the largest composite sample with unified scaling on mass estimates, however, we collect only large samples of clusters from the literature, with each having at least 10 overlapping common clusters with the other samples so that the estimated masses of these common clusters can be compared and scaled. For this purpose, we take six large samples from the literature: the X-ray cluster samples by Vikhlinin et al. (2009a, hereafter V09), Mantz et al. (2010, hereafter M10), Piffaretti et al. (2011, hereafter P11) and Takey et al. (2013, 2014, hereafter T14), and the SZ cluster samples from the Atacama Cosmology Telescope (ACT) survey by Hasselfield et al. (2013, hereafter H13) and the Planck survey by the Planck Collaboration et al. (2015, hereafter P15). We extract the cluster mass M_{500} from these references, which is the mass within a radius of r_{500} within which the mean density of a cluster is 500 times of the critical den-

sity of the universe, $\rho_c \equiv 3H^2(z)/8\pi G$, i.e.

$$M_{500} = \frac{4\pi}{3} r_{500}^3 \times 500 \rho_c. \tag{1}$$

In the following we briefly introduce the six samples:

V09: Vikhlinin et al. (2009a) estimated the total masses for 85 clusters at $z \approx 0.05$ and $z \approx 0.5$ by using high-quality *Chandra* observations. The cluster mass M_{500} was derived by using three X-ray proxies: average temperature T_X, gas mass M_{gas}, and $Y_X = T_X \times M_{\mathrm{gas}}$. Vikhlinin et al. (2009a) calibrated their scaling relations with cluster mass (Kravtsov et al. 2006) by using a sample of well–observed relaxed clusters at low redshifts. The mass estimates derived using the three proxies are well matched with very small scatters. We adopt the cluster mass M_{500} they derived from M_{gas} and the gas mass fraction, which depends weakly on cluster mass.

M10: Mantz et al. (2010) used high-quality *Chandra* observations to estimate the gas mass M_{gas} for 130 massive clusters that have 0.1-2.4 keV luminosity larger than 2.5×10^{44} erg s^{-1} in the redshift range of $0.05 < z < 0.88$. Different from V09, they derived the total mass M_{500} assuming a constant value of gas mass fraction.

P11: Piffaretti et al. (2011) compiled 1743 clusters in the redshift range of $z < 1.2$ from the ROSAT All Sky Survey-based data, including NORAS (Böhringer et al. 2000), REFLEX (Böhringer et al. 2004), BCS (Ebeling et al. 1998), SGP (Cruddace et al. 2002), NEP (Henry et al. 2006), MACS (Ebeling et al. 2001) and CIZA (Ebeling et al. 2002), and serendipitous searches in the ROSAT observations including 160SD (Mullis et al. 2003), 400SD (Burenin et al. 2007), SHARC (Romer et al. 2000), WARPS (Horner et al. 2008) and EMSS (Gioia et al. 1990). All clusters have their X-ray luminosity, $L_{X,500}$, measured within r_{500}. The cluster masses were estimated from $L_{X,500}$ by using the scaling relation between mass and X-ray luminosity obtained by Arnaud et al. (2010) and Pratt et al. (2009), with a typical uncertainty of 15%.

T14: Takey et al. (2013) presented a sample of 530 X-ray clusters selected from the XMM-Newton serendipitous source catalog in the SDSS sky region, of which 310 clusters have spectroscopic redshifts and are in the redshift range of $0.03 < z < 0.70$. Takey et al. (2014) updated the photometric redshifts of the clusters by using the SDSS DR10 spectroscopic data. Cluster masses are estimated by using the X-ray luminosity $L_{X,500}$ and the scaling relations given by Pratt et al. (2009).

H13: Hasselfield et al. (2013) presented a catalog of 68 clusters over $0.15 < z < 0.8$ detected via SZ effect at 148 GHz in the ACT survey. The authors provided cluster mass estimates for the 68 clusters near the celestial equator together with 23 clusters in the southern survey. Four different mass estimates were given in the paper based on the Compton parameter calibrated to the Universal Pressure Profile model (Arnaud et al. 2010), the Bode et al. (2012) model, the Nonthermal model (Trac et al. 2011) and the dynamical masses of Sifón et al. (2013), respectively. These four mass estimates are well correlated with different normalization. Here, we adopt the mass estimates calibrated to dynamical masses of Sifón et al. (2013).
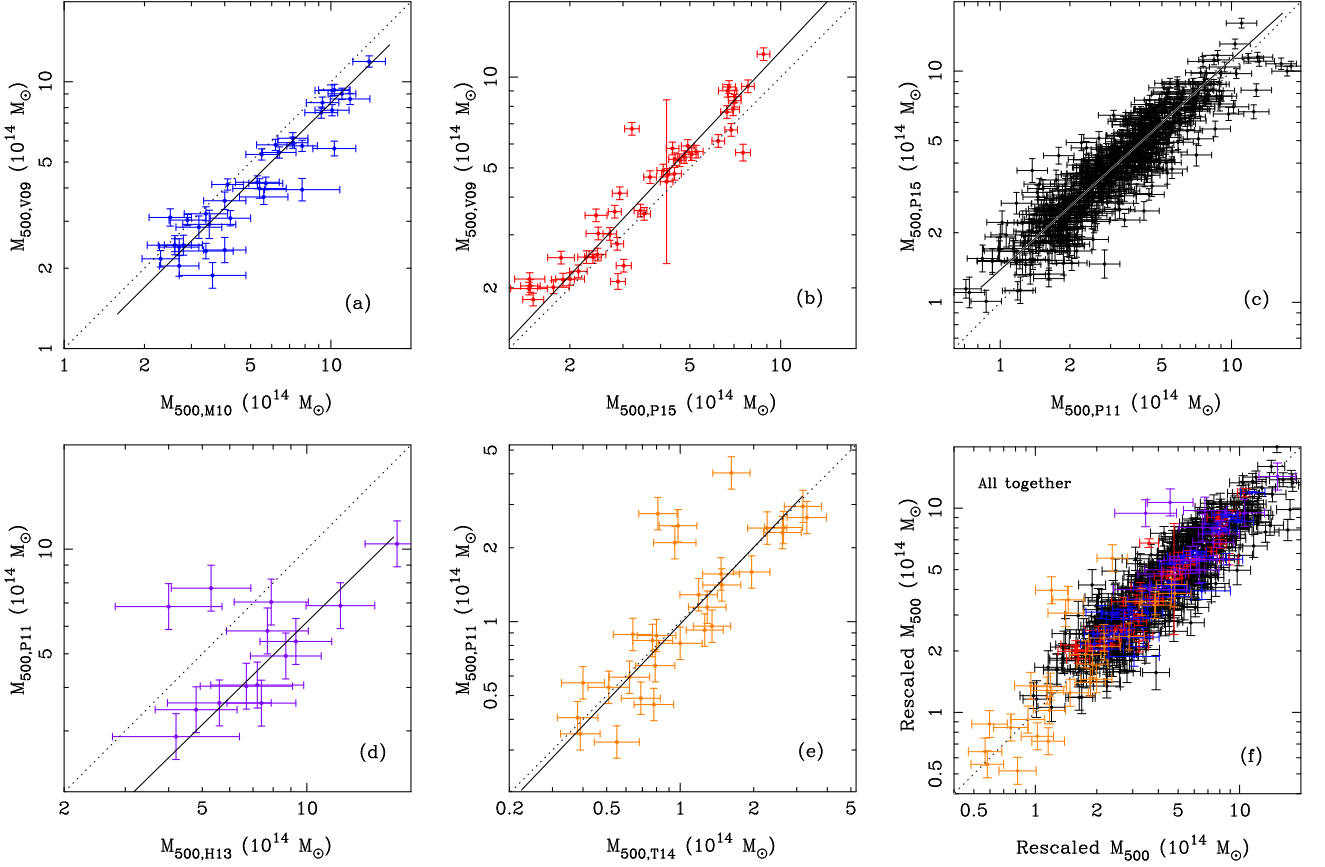
FIG. 1.— Comparison of the estimated masses for the overlapping common clusters in different samples from the literature. The solid line is the best fit, and the dotted line indicates the equivalence. All data in panels (a) – (e) are finally rescaled to V09 via the best fit(s), and summarized in panel (f), where the mass values in the X-axis are rescaled from the X-values of panels (a) – (e) and the mass values in the Y-axis are rescaled from the Y-values of panels (a) – (e). Because the intrinsic uncertainty of mass-observable relation is larger than 5% (Vikhlinin et al. 2009a), we here set the minimum uncertainty of 5% for cluster mass even though it could be formally small in the literature.

P15: The all-sky Planck catalog of clusters is the largest SZ-selected catalog to date, containing 1653 clusters with redshifts up to $z \sim 1$ in the second catalog (Planck Collaboration et al. 2015). Among these, 1203 clusters have counterparts in previous X-ray, optical, SZ, and infrared data and 1094 clusters have redshifts. The masses of the 1094 clusters with redshift information were derived by using the Compton parameter (Planck Collaboration et al. 2014).

The masses of galaxy clusters in these samples are compiled to form a very large composite sample. However, we notice that cluster masses in these six samples were estimated by using different mass proxies with different scaling relations, and even cluster masses derived from different X-ray proxies in the same sample are not consistent as well. Though both V09 and M10 derived cluster masses via the gas mass M_{gas}, normalization of the fraction of gas mass and dependence on cluster mass are different in the two papers. Different cluster masses are obtained in H13 if they are normalized to different models. Therefore, to get the uniformed scale for estimated masses of galaxy clusters in a composite sample, the mass estimates in different samples by different authors must be rescaled to each other for consistency.

In general, the mass estimates derived by the proxies of M_{gas} and Y_X are more reliable than those from the X-ray luminosity (Kravtsov et al. 2006). For the SZ clusters, we find that the mass estimates depend on model

for the ACT clusters (Hasselfield et al. 2013); the cluster masses from the Planck survey are probably systematically underestimated (Planck Collaboration et al. 2014; von der Linden et al. 2014a). In this work, we rescale cluster masses to the standard obtained by Vikhlinin et al. (2009a) because their mass estimates are based on very high-quality X-ray data and the mass proxy shows only a small scatter after careful calibration using the known masses of low redshift relaxed clusters.

The easy approach to rescale the cluster masses to the standard of Vikhlinin et al. (2009a) is to compare the mass values of common clusters that overlap in these different samples. As shown in Figure 1(a), cluster masses derived by V09 and M10 using the same proxy M_{gas} show a systematic offset. The best fit is found as

$$\log M_{500,\mathrm{V09}} = (0.99 \pm 0.06) \log M_{500,\mathrm{M10}} - (0.07 \pm 0.04).$$
(2)

This equation can be used to convert the mass estimates of all galaxy clusters in the M10 sample to the V09 standard. Similarly, we compare the mass estimates for overlapping common galaxy clusters in V09 and P15, as shown in Figure 1(b), and obtain the conversion equation as

$$\log M_{500,\mathrm{V09}} = (1.06 \pm 0.03) \log M_{500,\mathrm{P15}} + (0.02 \pm 0.02).$$
(3)

In the cluster sample of P11, there are too few clusters that overlap with V09 sample. However, there are many overlap-

TABLE 1
RESCALED MASS AND NEWLY CALCULATED RICHNESS FOR 1191 GALAXY CLUSTERS

ID	R.A. (deg)	Decl. (deg)	z	M_{500} ($10^{14}\ M_\odot$)	$\sigma_{M_{500}}$ ($10^{14}\ M_\odot$)	r_{500} (Mpc)	$\sigma_{r_{500}}$ (Mpc)	$R_{L*,500}$	Reference
(1)	(2)	(3)	(4)	(5)	(6)	(7)	(8)	(9)	(10)
1	0.49367	12.06612	0.1995	4.40	0.42	1.08	0.04	86.20	P11,P15
2	0.79826	−6.09169	0.2328	7.20	0.44	1.26	0.03	105.02	P11,P15
3	0.95698	2.06647	0.0967	2.57	0.26	0.94	0.03	60.13	P11,P15
4	1.24353	11.70091	0.0763	2.00	0.30	0.87	0.05	23.18	P11
5	1.34984	16.21926	0.1155	3.70	0.56	1.05	0.06	67.62	P11
6	1.58453	10.86429	0.1680	4.46	0.41	1.10	0.03	68.22	P11,P15
7	2.04332	2.02009	0.3665	6.44	0.70	1.16	0.04	68.70	H13,P15
8	2.33609	6.82309	0.2378	5.80	0.66	1.17	0.05	112.20	P15
9	2.51443	17.77082	0.1714	3.76	0.59	1.04	0.06	64.06	P15
10	2.57239	6.64203	0.2648	5.68	0.72	1.15	0.05	53.00	P15

Notes: Column (1): sequence number; Column (2) and (3): R.A. (J2000) and Decl. (J2000) of cluster; Column (4): spectroscopic redshift of cluster; Column (5) and (6): rescaled cluster mass M_{500} and its uncertainty $\sigma_{M_{500}}$; Column (7) and (8): recalculated cluster radius r_{500} and its uncertainty $\sigma_{r_{500}}$ from M_{500}; Column (9): newly defined cluster richness $R_{L*,500}$; Column (10): reference for original mass estimate: V09 for Vikhlinin et al. (2009a), M10 for Mantz et al. (2010), P11 for Piffaretti et al. (2011), H13 for Hasselfield et al. (2013), P15 for Planck Collaboration et al. (2015), T14 for Takey et al. (2013, 2014). (This table is available in its entirety in a machine-readable form in the online journal. A portion is shown here for guidance regarding the form and content.)

ping common clusters with the P15 catalog. We can rescale the cluster masses of the P11 sample to the P15 scale first, and then convert to the V09 standard. Comparing the mass estimates of the common clusters overlapping in the P11 and P15 samples shown in Figure 1(c) gives

$$\log M_{500,\mathrm{P15}} = (0.90 \pm 0.02) \log M_{500,\mathrm{P11}} + (0.15 \pm 0.01). \quad (4)$$

Combining the above two conversion equations, we get

$$\log M_{500,\mathrm{V09}} = (0.95 \pm 0.03) \log M_{500,\mathrm{P11}} + (0.18 \pm 0.02). \quad (5)$$

The H13 sample of the SZ clusters has even fewer overlaps with the samples of V09 and P15. However, there are some common clusters overlapping in the H13 and P11 samples. We compare their mass estimates as shown in Figure 1(d), and get

$$\log M_{500,\mathrm{P11}} = (0.98 \pm 0.30) \log M_{500,\mathrm{H13}} - (0.19 \pm 0.30). \quad (6)$$

When it is combined with Equation (5), we get the conversion equation to the V09 standard as

$$\log M_{500,\mathrm{V09}} = (0.93 \pm 0.29) \log M_{500,\mathrm{H13}} + (0.00 \pm 0.29). \quad (7)$$

The same holds for the clusters in the T14 sample. The best fit between the T14 mass and the P11 mass as shown in Figure 1(e) is

$$\log M_{500,\mathrm{P11}} = (1.04 \pm 0.08) \log M_{500,\mathrm{T14}} - (0.01 \pm 0.02), \quad (8)$$

and the conversion to the V09 standard is through

$$\log M_{500,\mathrm{V09}} = (0.99 \pm 0.08) \log M_{500,\mathrm{T14}} + (0.17 \pm 0.03). \quad (9)$$

The masses of clusters thus scaled in Figure 1(a)–(e) have excellent consistency, as shown in Figure 1(f), which shows a scatter of only 0.1 dex, i.e. $\sigma_{\log M_{500}} = 0.10$. Most of the galaxy clusters from the V09, M10, P11, H13, and P15 samples have a rescaled mass of $M_{500} > 2 \times 10^{14} M_\odot$, while clusters in the T14 sample often have a smaller mass of $0.3 \times 10^{14} M_\odot < M_{500} < 2 \times 10^{14} M_\odot$.

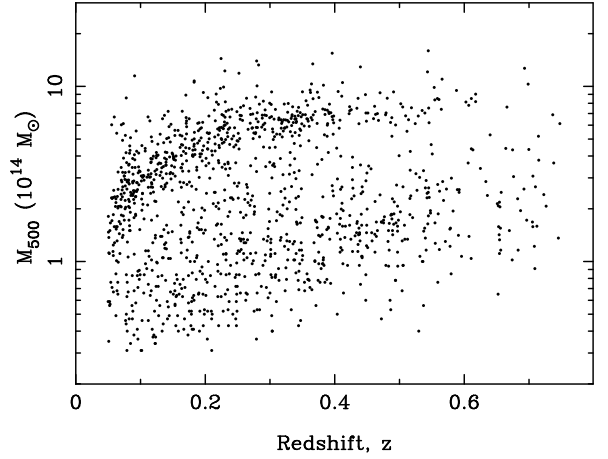The rescaled masses of the galaxy clusters from the six sam-

FIG. 2.— The masses for 1191 clusters in the composite calibration sample are in the range of $0.3 – 20 \times 10^{14}\ M_\odot$, and the redshifts are distributed up to 0.75.

ples will be used to calibrate the optical mass proxy, which will be derived from the SDSS data. Therefore we limit the composite sample to galaxy clusters in the SDSS sky region, which must have a spectroscopic redshift either in the NASA/IPAC Extragalactic Database or from the SDSS spectroscopic observations (Alam et al. 2015). We also limit the sample to a mass of $M_{500} > 0.3 \times 10^{14}\ M_\odot$ and in the redshift range of $0.05 < z < 0.75$. The lower redshift limit is set due to a photometry problem for very bright galaxies in the SDSS data, and the redshift upper limit is considered for the reliable detection of cluster galaxies in the SDSS data. We further visually inspect the color images[1] and exclude nine clusters that are seriously contaminated by very bright exposure-saturated stars. Finally we get 29, 64, 584, 50, 412, and 370 clusters from the V09, M10, P11, H13, T14 and P15 samples, respectively. After the overlapping common clusters are merged with their masses estimated from uncertainty-weighted average, the composite calibration sample consists
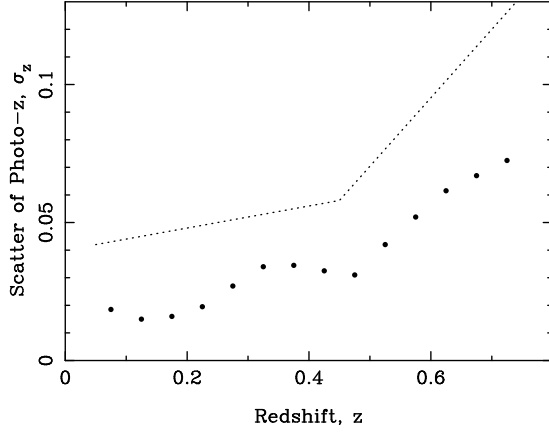
[1] http://skyserver.sdss.org/dr12/en/tools/chart/navi.aspx

FIG. 3.— Data scatter σ_z of photo-z varies with redshift, obtained from the comparison of spectroscopic redshifts and estimated photo-zs of a large SDSS galaxies. The dotted line represents the half thickness Δz of the photo-z slice defined by Equation (10) for discrimination of member galaxies.

of 1191 clusters, as listed in Table 1. The cluster radius r_{500} are re-estimated from the rescaled mass M_{500} by using Equation (1). The distributions of their masses and redshifts are shown in Figure 2.

2.2. *Optical luminosity and richness of galaxy clusters*

We discriminate the cluster member galaxies and calculate the total optical luminosity of clusters by using the SDSS spectroscopic and photometric data following our previous procedures in Wen et al. (2012, hereafter WHL12) but with a few improvements. The cluster richness is defined from the optical luminosity, which can act as the optical mass proxy for galaxy clusters.

2.2.1. *Discrimination of cluster member galaxies*

We only consider the bright member galaxies of $M_r^e(z) \leq -20.5$. Here, M_r^e is the evolution-corrected absolute magnitude in the r band, $M_r^e(z) = M_r(z) + Qz$. Assuming the passive evolution of a galaxy population formed at $z_f = 2$ (Lin et al. 2006; Crawford et al. 2009) and adopting a stellar population synthesis model (Bruzual & Charlot 2003) with the initial mass function of Chabrier (2003) and solar metallicity, we obtain the value of $Q \sim 1.16$ at redshift $z < 0.8$. The bright member galaxies of a cluster can be discriminated around a brightest cluster galaxy (BCG) in a small redshift range, i.e. a redshift slice.

To discriminate the cluster galaxies, the spectroscopic redshifts are taken if they are available in the SDSS DR12 (Alam et al. 2015); otherwise, photometric redshifts (photo-zs hereafter) will be used. For the objects classified as galaxies with only photo-zs, we remove those with deblending problems and those marked as 'SATURATED' using the flags[2], and also discard those objects with a large photo-z error $z\mathrm{Err} > 0.08(1 + z)$. These selection procedures remove most of the contamination from stars and galaxies with a bad photometry.

For galaxies with spectroscopic redshifts, only those within a redshift slice of $c\Delta z/(1+z) = 2500\,\mathrm{km\,s^{-1}}$ are considered as member galaxies. Here c is the speed of light, and z is the redshift of a cluster.

[2] (flags & 0x20) = 0 and (flags & 0x80000) = 0 and ((flags & 0x400000000000) = 0 or psfmagerr$_r$ <= 0.20) and ((flags & 0x40000) = 0)

For most member galaxies, their photo-zs were estimated by optical magnitudes in five bands of the SDSS and have an uncertainty much larger than those of spectroscopic redshift (Csabai et al. 2007). The data scatter of photo-z varies with redshift, as shown in Figure 3, and is smaller than 0.035 at a redshift of $z < 0.5$ but increases to $\sigma_z \sim 0.075$ at a redshift of $z > 0.7$. Only galaxies within the redshift slice of $z \pm \Delta z$ are considered as member galaxies of a cluster at a redshift of z. In Wen et al. (2009) and Wen et al. (2012) the half thickness of the slice is taken as $\Delta z = 0.04\,(1 + z)$, and the majority of the member galaxies can be well discriminated for clusters with a redshift of $z < 0.42$. However, due to the large uncertainty of photo-z, such a slice leads to incomplete recognizance of member galaxies for clusters at higher redshifts. Here we adopt the photo-z slice in the form of

$$\Delta z = \begin{cases} 0.04\,(1 + z) & \text{for } z \leq 0.45 \\ 0.248\,z - 0.0536 & \text{for } z > 0.45 \end{cases}, \quad (10)$$

which is about 1.75–2.00 σ_z and by which most cluster member galaxies can be identified up to a high redshift. Such a larger photo-z slice leads to a slightly higher completeness for identification of member galaxies but introduces more contamination.

Compared to Wen et al. (2012), we improve the discrimination of member galaxies in three aspects: (a) spectroscopic redshifts are considered for member galaxies; (b) the evolution of absolute magnitudes is improved from $Q = 1.62 \pm 0.30$ (Blanton et al. 2003) to the current value of $Q = 1.16$; and (c) the thickness of the photo-z slice at high redshifts is enlarged according to the photo-z scatter.

2.2.2. *Total r-band luminosity of cluster member galaxies and background estimation*

In general for each known cluster, the total r-band luminosity can be calculated by summing the luminosity of recognized member galaxies. The total luminosity is measured in units of L^* which is the evolved characteristic luminosity of galaxies in the r-band defined by $L^*(z) = L^*(0)10^{0.4Qz}$, here again $Q = 1.16$.

However, the contamination by background field galaxies has to be subtracted. To estimate the local background, we follow the method analogous to Popesso et al. (2004). For each cluster, we take the BCG as the center of a galaxy cluster, and then divide the annulus between 2–4 Mpc from the BCG into 48 sectors with equal areas. Within the same magnitude limit and the same photo-z slice, the field galaxies in these sectors fainter than the second brightest cluster member galaxies are used to calculate the background. We get the total r-band luminosity of bright galaxies in each sector, and estimate the mean and deviation σ. The sectors with a luminosity obviously deviating from the mean by more than 3σ are discarded, and the mean is recalculated for the local background which is scaled and subtracted from the total luminosity.

2.2.3. *Scaling relations between the optical data and mass*

The goal here is to establish the scaling relation between the cluster mass and the luminosity or richness derived from optical data. As shown by Wen et al. (2012), if there are merely optical survey data for a cluster, a few steps are needed to derive the richness from optical data: (1) discriminate cluster member galaxies and get their redshifts; (2) get the optical luminosity $L_{1\mathrm{Mpc}}$ from member galaxies within 1 Mpc, and then derive the cluster radius r_{500}; and (3) get the optical lu-
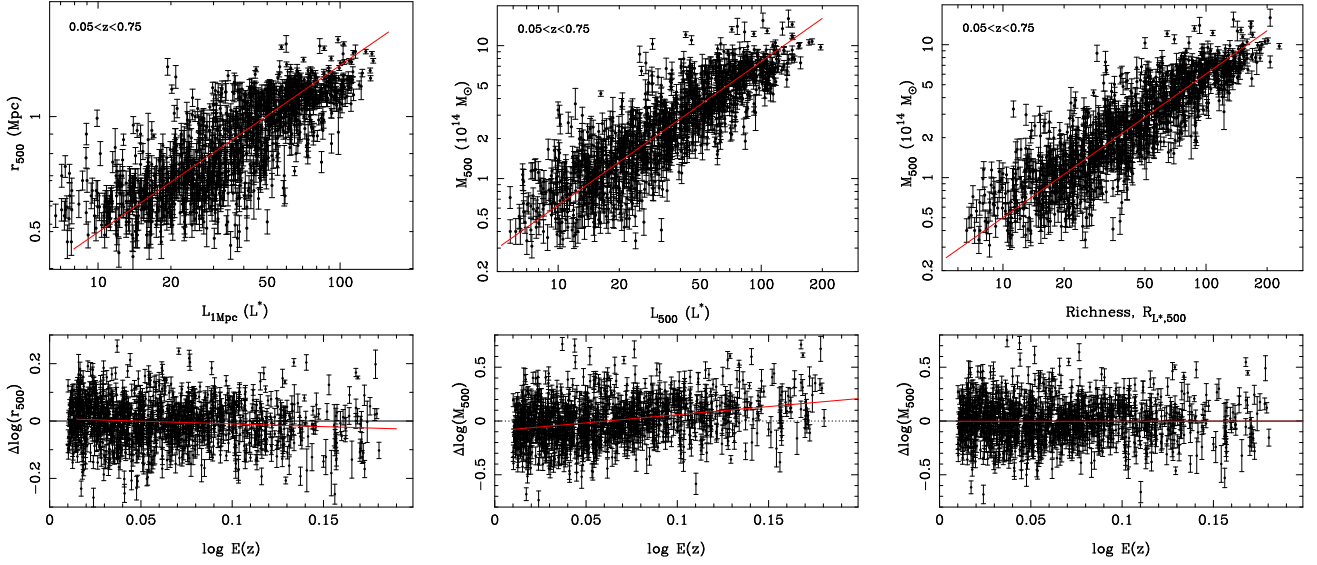
FIG. 4.— Upper panels are the scaling relations between cluster parameters derived from the optical data (the X-axis) and cluster radius or mass (the Y-axis) for the 1191 clusters from the composite calibration sample. The data scatters are plotted in the lower panels against $\log E(z)$ to check their possible evolution.

minosity L_{500} within r_{500}, and then the richness defined as $R_{L*,500} = L_{500}/L^*$.

First, to estimate r_{500} from optical data, we have to establish the relation between r_{500} and an optical observable that is the total r-band luminosity L_{1Mpc} (in units of L^*, with background subtracted) of member galaxies within 1 Mpc from the cluster center. As shown in the left panels of Figure 4, we find that the values of r_{500} (in Mpc) in Table 1 are well correlated with L_{1Mpc}. The uncertainty of L_{1Mpc} comes from the incompleteness of member galaxies and residual contamination of background galaxies, which is about 10% for rich clusters (Wen et al. 2009). By taking a typical uncertainty of 15% on L_{1Mpc} for all clusters, we find the best fit to the data as

$$\log r_{500} = (0.45 \pm 0.01) \log L_{1Mpc} - (0.76 \pm 0.01). \quad (11)$$

The slope obtained here is consistent with that in Wen et al. (2012).

Some authors have shown that the scaling relation between M_{500} (or r_{500}) and an optical observable (e.g., richness) may evolve with redshift (Lin et al. 2004; Andreon & Congdon 2014; Wiesner et al. 2015), for example, due to higher concentration of the light-to-mass profiles at lower redshifts (Gu et al. 2013). On the other hand, bright member galaxies of $M_e \leq -20.5$ are incomplete in the SDSS photometric data at $z > 0.45$, so that the total luminosity could be underestimated. The 1191 clusters in the composite calibration sample are in a very large redshift range, allowing us to clarify any redshift evolution of the scaling relations. For the scaling relation $r_{500} - L_{1Mpc}$, we calculate the deviation of r_{500} from the relation: $\Delta \log r_{500} = \log r_{500} - (0.45 \log L_{1Mpc} - 0.76)$ and find that $\Delta \log r_{500}$ is only slightly evolving with the redshift in the form of (see the lower left panel in Figure 4)

$$\Delta \log r_{500} = (-0.20 \pm 0.06) \log E(z) + (0.01 \pm 0.01), \quad (12)$$

where $E(z) = \sqrt{\Omega_\Lambda + \Omega_m (1+z)^3}$. Including this small correction, the radius r_{500} is related to L_{1Mpc} and z by

$$\log r_{500} = (0.45 \pm 0.01) \log L_{1Mpc} - (0.75 \pm 0.01)$$
$$- (0.20 \pm 0.06) \log E(z). \quad (13)$$

We calculate the total r-band luminosity L_{500} (also in units of L^*, with background subtracted) of member galaxies within the radius of r_{500} for the 1191 clusters by using the SDSS data. As shown in the upper middle panel of Figure 4, there exists excellent correlation between L_{500} and the cluster mass M_{500} (in units of $10^{14} M_\odot$), and the best fit is

$$\log M_{500} = (1.08 \pm 0.02) \log L_{500} - (1.28 \pm 0.02). \quad (14)$$

Again, to check for the possible evolution with redshift, the deviations of M_{500} from the above fitted relation, $\Delta \log M_{500} = \log M_{500} - (1.08 \log L_{500} - 1.28)$, are plotted against $E(z)$ in the middle lower panel of Figure 4, which shows a correlation in the form of

$$\Delta \log M_{500} = (1.51 \pm 0.14) \log E(z) - (0.09 \pm 0.01), \quad (15)$$

Though the total r-band luminosity L_{500} in principle may slightly be underestimated for clusters of $z > 0.45$ (i.e., $\log E(0.45) = 0.104$), the $\Delta \log M_{500}$ has to be so corrected. We then can define the richness of the galaxy cluster from the total r-band luminosity L_{500}, which can act as a well-calibrated mass proxy in the optical band, as

$$R_{L*,500} = L_{500} E(z)^{1.40}. \quad (16)$$

Such a richness is independent of redshift and is valid in the redshift range of $0.05 < z < 0.75$, as shown in the right panels of Figure 4. The thus-calculated richness $R_{L*,500}$ for galaxy clusters in the composite calibration sample is listed in Table 1. The scaling relation between the cluster mass and the richness is

$$\log M_{500} = (1.08 \pm 0.02) \log R_{L*,500} - (1.37 \pm 0.02), \quad (17)$$

which is consistent with but more accurate than the mass–richness relation obtained in our previous work (Wen et al. 2012) and the $M_{500} - \lambda$ relation given by Rykoff et al. (2012). The scatter of mass values is about 0.17 dex, i.e. $\sigma_{\log M_{500}} = 0.17$. Taking out the inherent scatter $\sigma_{\log M_{500}} = 0.10$ of the rescaled masses of the composite calibration sample, the mass uncertainty estimated by $R_{L*,500}$ should be $\sigma_{\log M_{500}} = 0.14$.

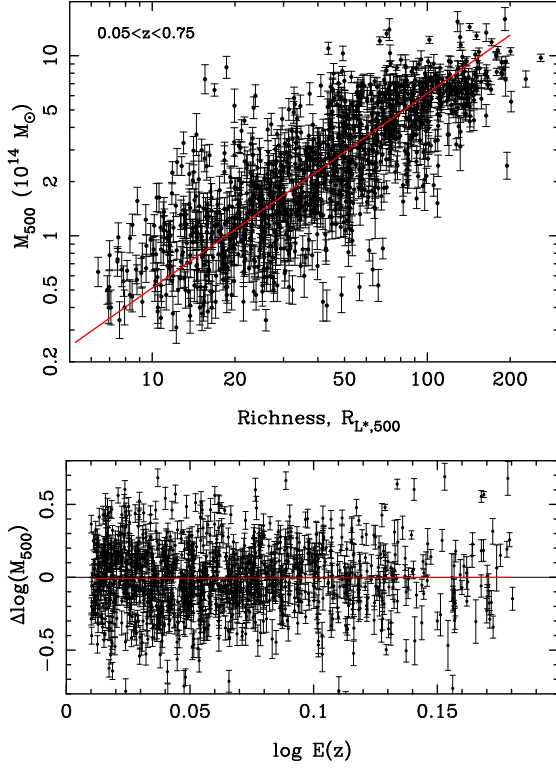Because clusters in the composite calibration sample are

FIG. 5.— Correlation between M_{500} and the directly optically estimated $R_{L*,500}$ for the 1191 clusters in Table 1. Different from the right panel of Figure 4, the values of r_{500} and $R_{L*,500}$ are both estimated from merely optical data.

distributed in a wide range of mass and redshift, the scaling relations we derived above should be valid for clusters in the SDSS in the redshift ranges of $0.05 < z < 0.75$ with a mass of $M_{500} > 0.3 \times 10^{14}\ M_\odot$.

2.3. *Goodness of optical mass proxies*

How good is the richness $R_{L*,500}$ estimated from just the optical data (i.e., r_{500} is unknown previously) acting as a mass proxy? To get a quantitative estimate, we estimated the L_{1Mpc} of 1191 clusters in the composite calibration sample, and then get r_{500} from the scaling relation in Equation (13) so that L_{500} and hence $R_{L*,500}$ can be estimated from the member galaxies within r_{500}. Obviously the uncertainty of estimated r_{500} is propagated to L_{500} and then $R_{L*,500}$. The plot for M_{500} and $R_{L*,500}$ in Figure 5 shows a mass scatter in 0.20 dex, i.e. $\sigma_{\log M_{500}} = 0.20$. Taking out the inherent scatter of $\sigma_{\log M_{500}} = 0.10$ for the masses estimated from the X-ray and SZ observations, the mass scaled by $R_{L*,500}$ should have a scatter of $\sigma_{\log M_{500}} = 0.17$.

Can the richness in other cluster catalogs be used as a mass proxy? If so, how good is it? To find out the answer to these questions, we investigate the optical richness based on photometric data in the cluster catalogs of the maxBCG (Koester et al. 2007), the Gaussian Mixture Brightest Cluster Galaxy (GMBCG, Hao et al. 2010), the adaptive matched filter (AMF, Szabo et al. 2011), the WHL12 (Wen et al. 2012), the red-sequence Matched-filter Probabilistic Percolation (redMapper, Rykoff et al. 2014), the Cluster finding Algorithm based on Multi-band Identification of Red-sequence galaxies (CAMIRA, Oguri 2014), and the richness based on spectroscopic data by Yang et al. (2007) and

Tempel et al. (2014).

The richness is defined as the total number of galaxies in the catalogs of maxBCG, GMBCG, and redMapper, or defined as the total luminosity of member galaxies in the catalogs of the AMF and WHL12. Yang et al. (2007) adopted the characteristic luminosities or the characteristic stellar masses as the halo mass proxy of galaxy group/clusters, and here we take the halo mass for comparison. Tempel et al. (2014) provided the dynamical mass estimates based on radial velocity dispersion of member galaxies, which we will take for comparison.

We cross-match the galaxy clusters in Table 1 with clusters in the above cluster catalogs, and get the matched clusters within a projected distance of r_{500} and a redshift difference of 0.05. If more than one cluster in a catalog matches with a cluster in Table 1, we take the one with the minimum projected distance. Note that for different cluster catalogs, we take the redshift ranges up to their redshift distribution peaks. As shown in Table 2, we get different numbers of matched clusters for different catalogs. We estimate the cluster mass by using each richness and get the scatter of the mass. For comparison, the mass scatter for the same sample of matched clusters for each catalog is also calculated by using our newly defined richness. We find that the richness defined in this paper and those in redMapper and CAMIRA are equally good to act as optical mass proxy. The improvement in this paper is that the newly defined richness has the redshift evolution corrected and is good for a wide range of redshifts up to $z \sim 0.75$.

3. UPDATE OF THE WHL12 CLUSTER CATALOG

We identified 132,684 galaxy clusters by using the photo-z of galaxies from SDSS DR8 (Wen et al. 2012). Clusters were identified if they have a richness ≥ 12 and the number of member galaxies $N_{200} \geq 8$ within a radius of r_{200}. Here, r_{200} is the radius within which the mean density of a cluster is 200 times of the critical density of the universe. The cluster richness R_{L*} was defined to be the r-band total luminosity (in units of L^*) of member galaxies with $M_r^e \leq -20.5$ within r_{200}.

Two reasons lead us to update the WHL12 cluster catalog. First, the latest SDSS DR12 (Alam et al. 2015) released spectroscopic redshifts for about 2.30 million galaxies, of which about 1.35 million are luminous red galaxies (LRGs). In general LRGs are massive galaxies, and many of them are the BCGs or the bright member galaxies of clusters in the WHL12. We can update these spectroscopic redshifts for most of the WHL12 clusters. Second, the newly defined richness can act as an excellent mass proxy, and should be calculated for all clusters in the WHL12 catalog. In addition, by using the SDSS DR12 data, we can find rich galaxy clusters at high redshifts.

3.1. *Update on spectroscopic redshifts and the BCGs*

In general, we take the spectroscopic redshift of the BCG $z_{s,BCG}$ as the redshift of a cluster. SDSS DR12 has spectroscopic redshifts for about 2.30 million galaxies (Alam et al. 2015). Simple cross-matching the BCGs of the WHL12 clusters with the galaxies with spectroscopic data in the SDSS DR12 gives the redshifts for 84,760 (64%) clusters.

We then try to get spectroscopic redshifts of bright member galaxies. For clusters with available $z_{s,BCG}$, we consider only galaxies within $r_{500} = 2/3\, r_{200}$ from the BCG and within 2500 km s^{-1} from $z_{s,BCG}$ in the rest frame. Here r_{200} can be found in Table 1 of Wen et al. (2012). For clusters without

TABLE 2
COMPARISON OF DATA SCATTER FOR MASSES ESTIMATED FROM DIFFERENT RICHNESSES IN DIFFERENT CLUSTER CATALOGS.

Cluster catalog	Redshift range for matching	Number of matched clusters	$\sigma_{\log M_{500}}$ scaled from ref.	$\sigma_{\log M_{500}}$ from this work
maxBCG	$0.10 < z < 0.30$	325	0.29	0.20
GMBCG	$0.10 < z < 0.37$	502	0.27	0.19
AMF	$0.05 < z < 0.38$	402	0.26	0.20
WHL12	$0.05 < z < 0.42$	799	0.24	0.20
redMapper	$0.08 < z < 0.55$	610	0.17	0.18
CAMIRA	$0.1 < z < 0.6$	647	0.18	0.19
Yang et al.	$z < 0.2$	195	0.56	0.19
Tempel et al.	$z < 0.2$	149	0.23	0.19
This paper	$0.05 < z < 0.75$	1191	–	0.20

FIG. 6.— Distribution of the newly defined richness $R_{L*,500}$ for the WHL12 clusters.
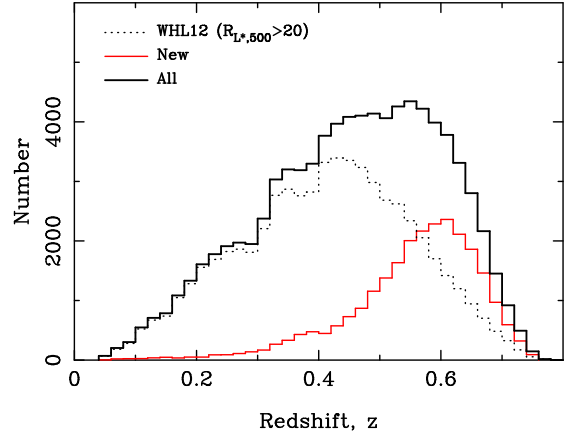

FIG. 7.— Redshift distribution of the newly identified clusters, compared with the WHL12 clusters of $R_{L*,500} \geq 20$ in the SDSS spectroscopic survey region.

$z_{\rm s,BCG}$, we consider the galaxies within $r_{500} = 2/3\,r_{200}$ from the BCGs and within a redshift difference of $0.03(1+z)$ from $z_{\rm p}$, the photo-z of clusters in Wen et al. (2012). This small redshift difference is about 2.0–2.5 times the uncertainty of the cluster photo-z. The mean spectroscopic redshifts of the member galaxies (including the BCG) is regarded to be the spectroscopic redshift of a cluster. Through this process, we get spectroscopic redshifts for 95,684 clusters, which is about 72% in the WHL catalog. In the SDSS spectroscopic survey region, 85% of the WHL clusters have spectroscopic redshifts obtained. Clusters located at low Galactic latitudes have no spectroscopic redshifts yet.

The position and the BCG have been updated for some clusters as well. In Wen et al. (2012), all objects with the deblending problems or marked as "SATURATED" (see the flags in Section 2.2) were removed from the photometric data in the procedure for identifying galaxy clusters. The true BCGs that have such a flag or catastrophic photo-z have now been included by using the spectroscopic redshifts. If a galaxy is brighter than the BCG of an original WHL12 cluster within r_{200} and has a redshift difference of $0.03(1 + z)$ and is surrounded by other member galaxies in the SDSS color image, we take it to be the new BCG of the cluster. We hence update the BCGs for 3128 clusters.

3.2. *Update on cluster richness*

By using the scaling relations we obtained in Section 2.2.3, we update the richness of galaxy clusters in the WHL12 catalog via the following steps:

$$L_{1\rm Mpc} \rightarrow r_{500} \rightarrow L_{500} \rightarrow R_{L*,500} \ .$$

That is to say, we have to estimate r_{500} from $L_{1\rm Mpc}$, and then get L_{500} and $R_{L*,500}$.

The updated parameters are listed in Table 3, where the cluster names, coordinates of the BCG, cluster redshift, and the r-band magnitude, as well as the newly estimated radius r_{500} and newly defined richness $R_{L*,500}$ are listed. The number of member galaxies N_{500} within r_{500} and the number of these galaxies with spectroscopic redshifts $N_{500,\rm sp}$ are given for reference. The distribution of $R_{L*,500}$ is shown in Figure 6; it has a peak around $R_{L*,500} = 20$. We noticed that 5183 clusters in the WHL12 catalog has a low new richness of $R_{L*,500} < 8$.

3.3. *Complementary galaxy clusters at high redshifts*

Identification of galaxy clusters at high redshifts was incomplete due to the large uncertainty of the photometric redshift, so that the the number of clusters in the WHL12 catalog drops down at redshifts of $z > 0.42$ (Wen et al. 2012, see also Figure 7). Here we identify complementary rich clusters around bright galaxies which have spectroscopic redshifts measured in the SDSS DR12, with following procedures:

TABLE 3
THE WHL12 CLUSTER CATALOG WITH UPDATED PARAMETERS

Cluster name	R.A. (deg)	Decl. (deg)	z_p	z_s	r_{BCG}	r_{200} (Mpc)	R_{L*}	N_{200}	r_{500} (Mpc)	$R_{L*,500}$	$N_{500,sp}$	N_{500}
(1)	(2)	(3)	(4)	(5)	(6)	(7)	(8)	(9)	(10)	(11)	(12)	(13)
WHL J000000.6+321233	0.00236	32.20925	0.1274	−1.0000	14.92	1.72	70.63	24	1.01	68.28	0	19
WHL J000002.3+051718	0.00957	5.28827	0.1696	0.1694	16.20	0.94	17.48	9	0.72	24.46	1	9
WHL J000003.1−033245*	0.01276	−3.54578	0.5968	0.5973	20.14	1.00	19.19	11	0.83	49.33	2	13
WHL J000003.3+311354	0.01377	31.23175	0.5428	0.5293	20.17	0.87	14.27	8	0.63	25.43	2	9
WHL J000003.5+314708	0.01475	31.78564	0.0932	0.0916	15.18	0.94	16.97	9	0.69	21.14	1	11
WHL J000004.7+022826	0.01945	2.47386	0.4179	−1.0000	19.32	0.95	13.71	10	0.54	6.60	0	3
WHL J000005.5+354610	0.02303	35.76957	0.4762	−1.0000	19.59	0.91	15.58	9	0.63	19.13	0	6
WHL J000006.0+152548	0.02482	15.42990	0.1656	0.1731	16.60	1.13	23.53	19	0.79	19.53	2	12
WHL J000006.3+221220	0.02643	22.20558	0.3985	−1.0000	19.36	0.84	12.73	11	0.52	11.92	0	7
WHL J000006.6+100648	0.02755	10.11333	0.3676	0.3747	19.07	0.93	16.73	13	0.70	23.52	2	12

Note. Column (1): Cluster name, the name with '*' means the BCG is updated; Column (2) and (3): R.A. (J2000) and Decl. (J2000) of cluster; Column (4): photometric redshift of cluster; Column (5): spectroscopic redshift of cluster, −1.0000 means not available; Column (6): r-band magnitude of the BCG; Column (7): original r_{200} of cluster (Mpc); Column (8): original richness; Column (9): original number of member galaxy within r_{200}; Column (10): cluster radius r_{500} derived from optical luminosity; Column (11): newly defined cluster richness, $R_{L*,500}$; Column (12): number of member galaxies with spectroscopic redshifts within r_{500}; Column (13): number of all member galaxies within r_{500}. Column (4) and (7)–(9) are from Wen et al. (2012), Column (10)–(13) are derived in this paper.
(This table is available in its entirety in a machine-readable form in the online journal. A portion is shown here for guidance regarding the form and content.)

TABLE 4
NEWLY IDENTIFIED RICH CLUSTERS AT HIGH REDSHIFTS

Cluster name	R.A. (deg)	Decl. (deg)	z	r_{BCG}	r_{500} (Mpc)	$R_{L*,500}$	$N_{500,sp}$	N_{500}
(1)	(2)	(3)	(4)	(5)	(6)	(7)	(8)	(9)
WH J000004.2+021941	0.01743	2.32800	0.6443	20.15	0.69	27.88	1	6
WH J000004.3−091120	0.01809	−9.18902	0.6028	19.95	0.70	34.93	1	7
WH J000005.9+100144	0.02452	10.02896	0.6712	20.46	0.65	27.84	1	6
WH J000006.8+195244	0.02824	19.87897	0.4771	19.88	0.62	22.75	2	7
WH J000007.7+234443	0.03208	23.74541	0.5285	19.84	0.65	27.25	2	7
WH J000008.2+263228	0.03423	26.54098	0.5462	20.02	0.64	26.35	1	8
WH J000008.6+053257	0.03568	5.54922	0.5742	20.05	0.73	34.66	3	10
WH J000009.9−072520	0.04132	−7.42227	0.5847	20.78	0.62	24.19	1	8
WH J000010.4+041038	0.04318	4.17714	0.6954	21.29	0.58	24.96	1	6
WH J000013.5−022138	0.05613	−2.36069	0.4959	19.94	0.61	22.55	2	7

Note. Column (1): cluster name; Column (2) and (3): R.A. (J2000) and Decl. (J2000) of cluster; Column (4): spectroscopic redshift of cluster; Column (5): r-band magnitude of the BCG; Column (6): cluster radius r_{500} derived from optical luminosity $L_{1 \, Mpc}$; Column (7): cluster richness, $R_{L*,500}$; Column (8): number of member galaxies with spectroscopic redshifts within r_{500}; Column (9): number of all member galaxies within r_{500}.
(This table is available in its entirety in a machine-readable form in the online journal. A portion is shown here for guidance regarding the form and content.)

1. Get the spectroscopic redshift of a cluster candidate. Each bright galaxy of $M_e \leq -20.5$ with a spectroscopic redshift is assumed to be a member galaxy of a cluster candidate. All galaxies within 0.5 Mpc from a given galaxy and with a velocity difference in the rest frame less than 2500 km s^{-1} are taken to be the member galaxies of the cluster candidate. Then the redshift of the cluster is defined as the median value of the spectroscopic redshifts of these galaxies.

2. Determine the BCG. Generally, the true BCG, because it is the brightest, should have been observed in the spectroscopic survey already. However, the BCGs in some clusters may be not observed spectroscopically because of their blue colors (Crawford et al. 1999; Pipino et al. 2011) or the fiber collision limitation in the SDSS spectroscopic survey. The BCG candidates are the galaxies within 0.5 Mpc and with a velocity difference less than 2500 km s^{-1} from the target galaxy or with a photo-z difference of $0.03(1 + z)$. The small slice of photo-z is used here for the BCG selection to reduce contamination from field galaxies. The BCG of a cluster can-

didate is recognized as the brightest galaxy of these galaxies.

3. Calculate the richness and judge a rich cluster. After we have the redshift of a cluster candidate and also the recognized BCG, we then find the bright member galaxies in the redshift slice defined by Equation 10, as described in Section 2.2.3, and then calculate L_{1Mpc} to estimate r_{500}, and then get L_{500} and finally $R_{L*,500}$. We only identify rich clusters with a richness of $R_{L*,500} \geq 20$ (beyond the peak in Figure 6) and the number of bright galaxies within r_{500}, $N_{500} \geq 6$.

4. Clean the entries. It is possible that one rich cluster can be recognized two or more times in the above procedures when targeting different bright galaxies, and hence some entries should be merged to one cluster if their redshift difference is less than 0.1 and a projected distance is less than $1.5 \, r_{500}$.

We find 79,498 clusters through the above procedures, of which 54,079 can match the clusters in the WHL12 catalog with a redshift difference of 0.1 and a projected distance of $1.5 \, r_{500}$. The remaining 25,419 are newly identified clusters,
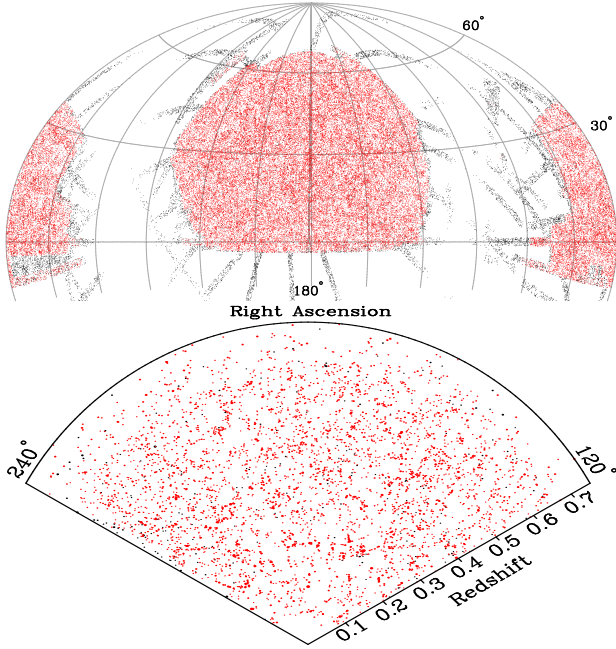
FIG. 8.— Sky coverage of rich clusters of $R_{L*,500} \geq 20$ (upper panel) and their radial distribution in a slice $0° \leq \text{Decl.} \leq 5°$ (lower panel). The red points are clusters with spectroscopic redshifts. The dot size in the lower panel is scaled by $\sqrt{R_{L*,500}}$.

all of them are limited to the SDSS sky coverage to obtain the optical spectroscopic and photometric data.

We established the scaling relations between the total r-band optical luminosity of member galaxies $L_{1\text{Mpc}}$ within 1 Mpc and the cluster radius (r_{500}). After correcting for weak redshift dependence, the scaling relation can be used to estimate the cluster radius from optical data. The cluster mass M_{500} is found to be well-correlated with the total r-band luminosity L_{500}, which evolves significantly with redshift. Considering the redshift evolution, we defined the new cluster richness as $R_{L*,500} = L_{500} E(z)^{1.40}$, which can be used as a mass proxy independent of redshift and is valid in the redshift range of $0.05 < z < 0.75$. The scatter of mass estimates is about 0.17 dex.

We updated the spectroscopic redshifts for the WHL12 clusters using the SDSS DR12 spectroscopic data, and then obtain their newly defined richness. We identify 25,419 complementary clusters at high redshifts around bright galaxies with a spectroscopic redshift in the SDSS DR12. The finial combined catalog contains 158,103 clusters in total, and about 89% of them have spectroscopic redshifts in the SDSS spectroscopic survey region.

as listed in Table 4. Most of them have a high redshift of $z > 0.4$ as shown in Figure 7.

If we combine the cluster sample in the updated WHL12 catalog and the complementary catalog of newly identified 25,419 clusters, we get 158,103 clusters, of which 96,257 have a richness of $R_{L*,500} \geq 20$. Figure 8 shows the sky coverage and radial distribution in a sky slice for clusters in the combined catalog. In the SDSS spectroscopic survey region, 89% of clusters have spectroscopic redshifts.

4. CONCLUSIONS

In this paper, we calibrated the optical mass proxy of galaxy clusters and applied it to update the WHL12 cluster catalog.

We collected clusters with known masses (M_{500}) derived from X-ray or SZ measurements from the literature, and rescaled them for consistency. The composite mass calibration sample consists of 1191 clusters in the redshift range $0.05 < z < 0.75$ with mass $M_{500} > 0.3 \times 10^{14} \ M_{\odot}$, and

REFERENCES

Alam, S., Albareti, F. D., Allende Prieto, C., et al. 2015, arXiv:1501.00963
Allen, S. W., Evrard, A. E., & Mantz, A. B. 2011, ARA&A, 49, 409
Andreon, S., & Congdon, P. 2014, A&A, 568, A23
Arnaud, M., Pratt, G. W., Piffaretti, R., et al. 2010, A&A, 517, A92
Bardeau, S., Soucail, G., Kneib, J.-P., et al. 2007, A&A, 470, 449
Berlind, A. A., Frieman, J., Weinberg, D. H., et al. 2006, ApJS, 167, 1
Bird, C. M. 1995, ApJ, 445, L81
Blanton, M. R., Hogg, D. W., Bahcall, N. A., et al. 2003, ApJ, 592, 819
Bode, P., Ostriker, J. P., Cen, R., & Trac, H. 2012, arXiv:1204.1762
Böhringer, H., Voges, W., Huchra, J. P., et al. 2000, ApJS, 129, 435
Böhringer, H., Schuecker, P., Guzzo, L., et al. 2004, A&A, 425, 367
Brunetti, G., Cassano, R., Dolag, K., & Setti, G. 2009, A&A, 507, 661
Bruzual, G., & Charlot, S. 2003, MNRAS, 344, 1000
Burenin, R. A., Vikhlinin, A., Hornstrup, A., et al. 2007, ApJS, 172, 561
Carlstrom, J. E., Holder, G. P., & Reese, E. D. 2002, ARA&A, 40, 643
Chabrier, G. 2003, PASP, 115, 763
Crawford, C. S., Allen, S. W., Ebeling, H., Edge, A. C., & Fabian, A. C. 1999, MNRAS, 306, 857

Crawford, S. M., Bershady, M. A., & Hoessel, J. G. 2009, ApJ, 690, 1158
Cruddace, R., Voges, W., Böhringer, H., et al. 2002, ApJS, 140, 239
Csabai, I., Dobos, L., Trencséni, M., et al. 2007, Astronomische Nachrichten, 328, 852
Dahle, H. 2006, ApJ, 653, 954
Dawson, K. S., Schlegel, D. J., Ahn, C. P., et al. 2013, AJ, 145, 10
Ebeling, H., Edge, A. C., Bohringer, H., et al. 1998, MNRAS, 301, 881
Ebeling, H., Edge, A. C., & Henry, J. P. 2001, ApJ, 553, 668
Ebeling, H., Mullis, C. R., & Tully, R. B. 2002, ApJ, 580, 774
Eisenstein, D. J., Annis, J., Gunn, J. E., et al. 2001, AJ, 122, 2267
Finoguenov, A., Reiprich, T. H., & Böhringer, H. 2001, A&A, 368, 749
Gioia, I. M., Maccacaro, T., Schild, R. E., et al. 1990, ApJS, 72, 567
Girardi, M., Giuricin, G., Mardirossian, F., Mezzetti, M., & Boschin, W. 1998, ApJ, 505, 74
Gladders, M. D., & Yee, H. K. C. 2000, AJ, 120, 2148
Gu, L., Gandhi, P., Inada, N., et al. 2013, ApJ, 767, 157
Hao, J., McKay, T. A., Koester, B. P., et al. 2010, ApJS, 191, 254
Hasselfield, M., Hilton, M., Marriage, T. A., et al. 2013, JCAP, 7, 8

Henry, J. P., Mullis, C. R., Voges, W., et al. 2006, ApJS, 162, 304
Horner, D. J., Perlman, E. S., Ebeling, H., et al. 2008, ApJS, 176, 374
Koester, B. P., McKay, T. A., Annis, J., et al. 2007, ApJ, 660, 239
Kravtsov, A. V., Vikhlinin, A., & Nagai, D. 2006, ApJ, 650, 128
Lin, Y.-T., Mohr, J. J., Gonzalez, A. H., & Stanford, S. A. 2006, ApJ, 650, L99
Lin, Y.-T., Mohr, J. J., & Stanford, S. A. 2004, ApJ, 610, 745
Lupton, R., Gunn, J. E., Ivezić, Z., Knapp, G. R., & Kent, S. 2001, in Astronomical Society of the Pacific Conference Series, Vol. 238, Astronomical Data Analysis Software and Systems X, ed. F. R. Harnden, Jr., F. A. Primini, & H. E. Payne, 269
Mantz, A., Allen, S. W., Ebeling, H., Rapetti, D., & Drlica-Wagner, A. 2010, MNRAS, 406, 1773
Merchán, M. E., & Zandivarez, A. 2005, ApJ, 630, 759
Mullis, C. R., McNamara, B. R., Quintana, H., et al. 2003, ApJ, 594, 154
Oguri, M. 2014, MNRAS, 444, 147
Okabe, N., Takada, M., Umetsu, K., Futamase, T., & Smith, G. P. 2010, PASJ, 62, 811
Piffaretti, R., Arnaud, M., Pratt, G. W., Pointecouteau, E., & Melin, J.-B. 2011, A&A, 534, A109
Pipino, A., Szabo, T., Pierpaoli, E., MacKenzie, S. M., & Dong, F. 2011, MNRAS, 417, 2817
Planck Collaboration, Ade, P. A. R., Aghanim, N., et al. 2014, A&A, 571, A20
—. 2015, arXiv:1502.01598
Popesso, P., Biviano, A., Böhringer, H., & Romaniello, M. 2007, A&A, 464, 451
Popesso, P., Biviano, A., Böhringer, H., Romaniello, M., & Voges, W. 2005, A&A, 433, 431
Popesso, P., Böhringer, H., Brinkmann, J., Voges, W., & York, D. G. 2004, A&A, 423, 449
Pratt, G. W., Croston, J. H., Arnaud, M., & Böhringer, H. 2009, A&A, 498, 361

Reichardt, C. L., Stalder, B., Bleem, L. E., et al. 2013, ApJ, 763, 127
Reiprich, T. H., & Böhringer, H. 2002, ApJ, 567, 716
Romer, A. K., Nichol, R. C., Holden, B. P., et al. 2000, ApJS, 126, 209
Rozo, E., Rykoff, E. S., Koester, B. P., et al. 2009, ApJ, 703, 601
Rykoff, E. S., Koester, B. P., Rozo, E., et al. 2012, ApJ, 746, 178
Rykoff, E. S., Rozo, E., Busha, M. T., et al. 2014, ApJ, 785, 104
Sifón, C., Menanteau, F., Hasselfield, M., et al. 2013, ApJ, 772, 25
Stoughton, C., Lupton, R. H., Bernardi, M., et al. 2002, AJ, 123, 485
Strauss, M. A., Weinberg, D. H., Lupton, R. H., et al. 2002, AJ, 124, 1810
Szabo, T., Pierpaoli, E., Dong, F., Pipino, A., & Gunn, J. 2011, ApJ, 736, 21
Takey, A., Schwope, A., & Lamer, G. 2013, A&A, 558, A75
—. 2014, A&A, 564, A54
Tempel, E., Tamm, A., Gramann, M., et al. 2014, A&A, 566, A1
Trac, H., Bode, P., & Ostriker, J. P. 2011, ApJ, 727, 94
Vikhlinin, A., Kravtsov, A., Forman, W., et al. 2006, ApJ, 640, 691
Vikhlinin, A., Burenin, R. A., Ebeling, H., et al. 2009a, ApJ, 692, 1033
Vikhlinin, A., Kravtsov, A. V., Burenin, R. A., et al. 2009b, ApJ, 692, 1060
Voit, G. M. 2005, Reviews of Modern Physics, 77, 207
von der Linden, A., Mantz, A., Allen, S. W., et al. 2014a, MNRAS, 443, 1973
von der Linden, A., Allen, M. T., Applegate, D. E., et al. 2014b, MNRAS, 439, 2
Wen, Z. L., Han, J. L., & Liu, F. S. 2009, ApJS, 183, 197
—. 2010, MNRAS, 407, 533
—. 2012, ApJS, 199, 34
Wetzel, A. R., Tinker, J. L., & Conroy, C. 2012, MNRAS, 424, 232
Wiesner, M. P., Lin, H., & Soares-Santos, M. 2015, arXiv:1501.06893
Yang, X., Mo, H. J., van den Bosch, F. C., et al. 2007, ApJ, 671, 153
York, D. G., Adelman, J., Anderson, Jr., J. E., et al. 2000, AJ, 120, 1579
Zhang, Y.-Y., Finoguenov, A., Böhringer, H., et al. 2008, A&A, 482, 451
Zhao, H.-H., Jia, S.-M., Chen, Y., et al. 2013, ApJ, 778, 124